ACS Catalysis

pubs.acs.org/acscatalysis

Research Article

Framework for Optimizing Polymeric Supports for Immobilized Biocatalysts by Computational Analysis of Enzyme Surface Hydrophobicity

Héctor Sánchez-Morán, Luciana Rocha Barros Gonçalves, Daniel K. Schwartz,* and Joel L. Kaar*

Cite This: *ACS Catal.* 2023, 13, 4304−4315

Read Online

ACCESS | Metrics & More | Article Recommendations | Supporting Information

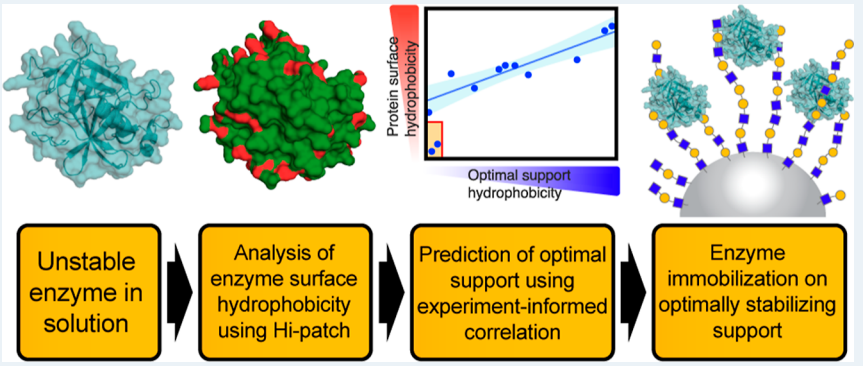

ABSTRACT: Immobilization is a powerful strategy for improving enzyme usability and stability in various technologies that employ biocatalysis. However, the interactions leading to stabilization or destabilization remain poorly understood, and a support that may stabilize one enzyme may destabilize another. Employing chemically heterogeneous and complex random copolymer brushes as supports, we demonstrate a rational approach toward estimating the chemical composition of an optimally stabilizing enzyme immobilization support by computational analysis of enzyme surface hydrophobicity. This approach was tested by immobilizing a range of enzymes with diverse functions and hydrophobicity on tunable statistical random copolymer brush supports composed of poly(ethylene glycol) methacrylate (PEGMA) and sulfobetaine methacrylate (SBMA). Remarkably, we observed greatly improved enzyme performance as a function of brush composition with enhancements in the retention of catalytic activity at temperatures as high as 90 °C. Additionally, we observed an increase in activity at the optimal temperature by as much as 20-fold relative to the activity at the optimal temperature of the unimmobilized form of the enzyme. Most significantly, our results showed that the optimal composition of the brush support correlated with the overall hydrophobicity of the enzyme surface ($\Delta G^{solv,total}$/area), which was determined from computational analysis. This correlation provides a framework for the choice of polymer brush supports based on enzyme structure and stabilizing enzymes using complex synthetic materials.

KEYWORDS: *biocatalysis, immobilization, enzyme stabilization, polymer brushes, enzyme engineering, protein surface hydrophobicity*

INTRODUCTION

The stabilization of surface-immobilized enzymes is a fundamental challenge due to the widespread importance of enzyme immobilization in various technologies, including biocatalysis,[1−3] biosensing,[4−6] and bioremediation.[7,8] This longstanding problem stems from our limited understanding of molecular mechanisms of inactivation and of the features of surfaces that damage or stabilize enzymes, respectively. Similarly, the understanding of how to rationally modify surfaces and materials to prevent enzyme inactivation has also remained elusive.[9,10] Currently, a common strategy in enzyme stabilization on surfaces involves attempting to minimize enzyme−surface interactions by using materials that are thought to be protein resistant. As such, it is common to passivate surfaces using putatively hydrophilic materials, including synthetic polymers [e.g., poly(ethylene glycol) (PEG)[11,12] and polyacrylamide],[13,14] biopolymers (e.g., agarose[15,16] and chitosan),[17,18] and proteins (e.g., BSA).[19,20] However, there is substantial evidence to suggest that even these materials may promote protein unfolding, contradicting the simplified paradigm that certain materials are universally stabilizing.[21−23]

Received: January 17, 2023
Revised: February 28, 2023

https://doi.org/10.1021/acscatal.3c00264
ACS Catal. 2023, 13, 4304−4315

Our recent work using single-molecule methods to study the stability of enzymes in contact with various materials has provided new insights into the complexity of the interactions between enzymes and surfaces. We specifically showed that these interactions are inevitable and that enzymes may be irreversibly unfolded/deactivated if they encounter anomalously strong denaturing sites, which are present on all surfaces.[24,25] Additionally, even when covalently tethered to surfaces, enzymes may be highly dynamic, undergoing rapid unfolding and re-folding, which impacts the mean folded fraction of the enzyme.[2,26] In addition to large-scale unfolding and re-folding, the activity of immobilized enzymes may also be affected by the magnitude of structural fluctuations (i.e., nanoscale motions) in the folded and unfolded states.[27]

Given these nuanced phenomena, it is interesting to consider how enzymes may be stabilized on surfaces by exploiting enzyme−surface interactions, rather than attempting to prevent them.[28] This idea has led to an alternative paradigm for designing materials that prevent unfolding and promote re-folding of denatured enzyme molecules. The materials identified to date that exhibit these properties are inherently chemically heterogeneous, highly tunable, and dynamic at molecular length scales.[29,30] For example, we have observed remarkable enhancements in the stability and activity of enzymes at elevated temperatures upon their immobilization to properly tuned random co-polymer brushes composed of poly(ethylene glycol) methacrylate (PEGMA) and sulfobetaine methacrylate (SBMA).[31] Notably, changes in the relative ratios of PEGMA-to-SBMA enable the hydrophobicity of the brush layer to be systematically varied.[32] Similarly, remarkable stability to chemical denaturants (e.g., urea) was observed using multicomponent lipid bilayers as supports for tethered enzymes.[33,34] The stabilizing effects of such materials are hypothesized to be due to their ability to preferentially self-assemble around the enzyme template. Specifically, the different chemical groups within the material may interact with patches of "like" properties on the enzyme surface. While reducing unfavorable interactions, self-assembly of the material may also promote re-folding by screening transiently exposed hydrophobic patches that induce misfolding and/or aggregation. Moreover, the enzyme may be stabilized via confinement effects, where the enzyme may be physically constrained from unfolding or aggregating due to preferential interactions with the material.

To better understand this approach, we previously investigated the potential correlation of the composition of random copolymer brush supports and the structural features of enzymes. Using several lipases, we found that the optimal ratio of PEGMA-to-SBMA copolymers could be estimated by a parameter that described the overall hydrophobic intensity of the enzyme surface, as calculated using a novel algorithm named "Hi-patch". Specifically, enzymes with greater surface hydrophobic intensity were stabilized on supports with greater hydrophobicity in the brush layer (i.e., comprising a higher fraction of PEGMA). While intriguing, this trend was demonstrated only for a small group of lipases and the extent to which this principle can be applied to other types of enzymes, including enzymes that are more hydrophilic and hydrophobic and with diverse structures and functions, remains unclear.

In this work, we sought to understand the extent to which the composition of mixed PEGMA/SBMA brushes can be tailored to a broad range of enzymes and can be used as the basis for strengthening design rules to rationally tune the brush composition for any enzyme. To develop this understanding, we selected a set of structurally and functionally diverse enzymes and characterized their stability as a function of brush composition under denaturing conditions. Using these enzymes, which had a broad range of surface hydrophobicity, we showed that there is a notable correlation between the optimal brush composition for each enzyme and their respective surface hydrophobic intensity, which was determined using Hi-patch. The results of this work demonstrate the potential of using the hydrophobicity of the enzyme surface as a metric to estimate the chemical composition of stabilizing support materials.

RESULTS AND DISCUSSION

Analysis of Enzyme Surface Hydrophobicity Using Hi-patch. To understand the extent to which the optimal chemistry of polymeric brush supports for any enzyme may be projected from the analysis of enzyme surface hydrophobicity, we studied the activity and stability of a set of structurally and functionally diverse enzymes. The enzymes used in this work comprised proteases (thrombin, trypsin, chymotrypsin, and subtilisin Carlsberg), an esterase (acetylcholinesterase, dAChE4), an aminoacylase (acylase I), a lyase (human carbonic anhydrase II, hCAII), and an oxidoreductase (horseradish peroxidase, HRP). Besides the diversity of functions, computational hydrophobicity analysis using the "Hi-patch" algorithm (summarized in Table 1) revealed that

Table 1. Protein Data Bank ID of Crystal Structure, Molecular Weight, and Overall Surface Hydrophobicity of Enzymes[a]

enzyme	PDB ID	molecular weight (kDa)	D_H[b] (nm)	$\Delta G^{solv,total}$/area (kJ/mol·nm^2)
thrombin[c]	[c]	35.5	5.05	−17.6
human carbonic anhydrase II (hCAII)	6B00	29.2	4.82	−17.2
acylase I[c,d]	[c]	45.3	6.29	−14.2
subtilisin Carlsberg	1SBC	27.4	4.61	−13.2
horseradish peroxidase (HRP)	1HCH	44.0	5.13	−13.0
chymotrypsin	4CHA	25.2	4.58	−13.0
trypsin	1UHB	23.8	4.44	−12.7
acetylcholinesterase (dAChE4)[d]	5HQ3	61.6	6.23	−11.2
Bacillus subtilis lipase A (LipA)[e]	1ISP	19.5	4.05	−15.5
Rhizomucor miehei lipase (RML)[e]	3TGL	29.6	4.75	−13.5
Candida rugosa lipase (CRL)[e]	1GZ7	57.5	6.02	−13.5
Candida antarctica lipase B (CALB)[e]	4K6G	33.5	5.07	−10.9

[a]The overall surface hydrophobicity ($\Delta G^{solv,total}$/area) of the monomeric form of each enzyme was determined using Hi-patch. Additionally, the reported molecular weights and hydrodynamic diameters (D_H) of the enzymes are for their respective monomeric forms. [b]Hydrodynamic diameters (D_H) were calculated using the HullRad online server, from ref 35. [c]Structure was predicted using AlphaFold2 as described in the Supporting Information. [d]Size and hydrophobicity calculations were computed using the monomeric form, despite their native existence in the dimeric form. [e]Values adapted from ref 31.

https://doi.org/10.1021/acscatal.3c00264
ACS Catal. 2023, 13, 4304−4315

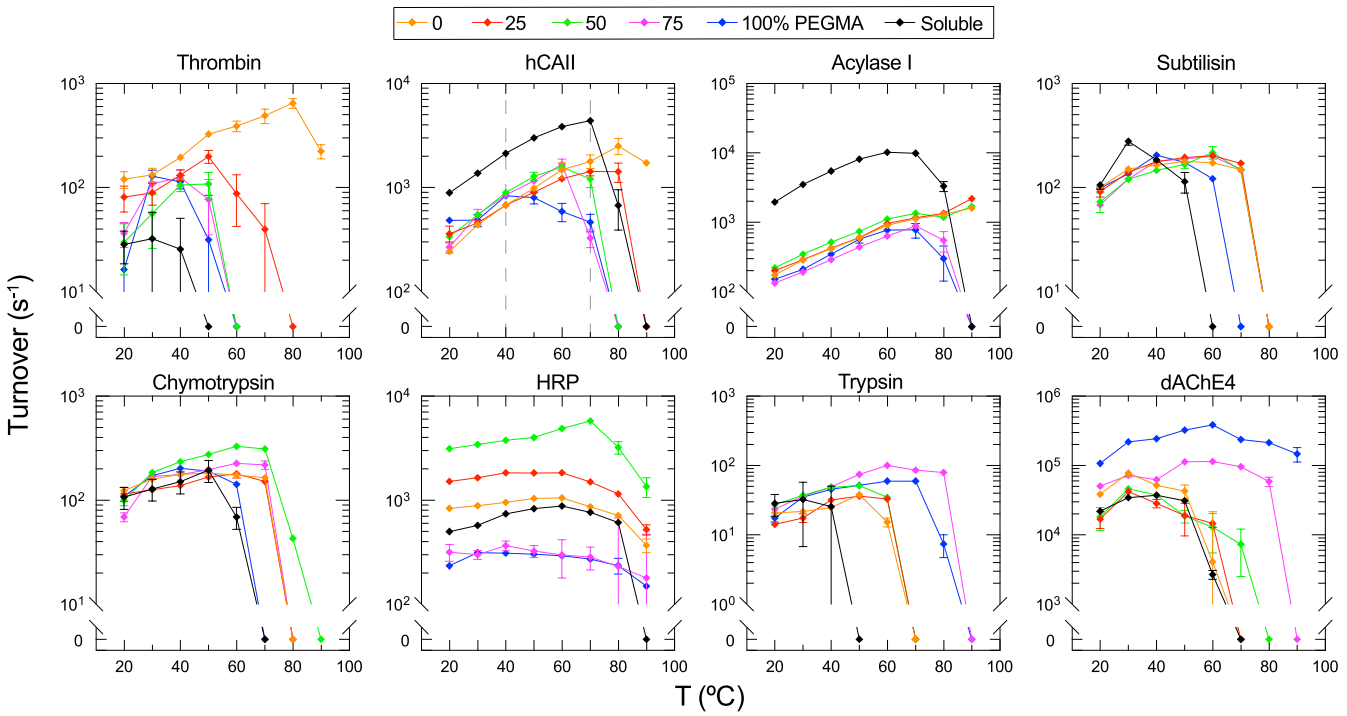

Figure 1. Temperature-dependent activity plots of immobilized and soluble enzymes. From top-left to bottom right, plots are ordered by increasing ΔG^{solv}/area based on the output of Hi-patch. Activity was measured by monitoring the initial rate of release of product as moles of product per mole of enzyme per second. Activities indistinguishable from background hydrolysis were represented as data points with a value of zero. Error bars represent the standard error of the mean for three technical replicates (n = 3).

these enzymes also spanned a wide range of surface hydrophobic intensities as measured by the overall free energy of solvation per area, ($\Delta G^{solv,total}$/area). Notably, the range of $\Delta G^{solv,total}$/area varied from −17.6 kJ/mol·nm^2 for thrombin, which is the most hydrophilic, to −11.2 kJ/mol·nm^2 for dAChE4, which is the most hydrophobic. For comparison, the $\Delta G^{solv,total}$/area of dAChE4 is similar to that of *Candida antarctica* lipase B (−10.9 kJ/mol·nm^2) that we characterized previously on mixed PEGMA/PSBMA brushes. While dAChE4 is difficult to produce recombinantly in *Escherichia coli*, we were able to produce sufficient yields to quantify its activity and stability upon immobilization, given that this variant of acetylcholinesterase has been optimized for expression in *E. coli*.[36] Additionally, for analysis using Hi-patch, we used the monomeric form of each enzyme despite the fact that some of the enzymes (e.g., dAChE4 and acylase I) exist as dimers natively in solution. The monomeric forms of dAChE4 and acylase, which have active sites distal to the dimeric interface, were used since the conditions used for immobilization allowed disruption of the dimers of each enzyme (e.g., via adding the non-ionic surfactant). While useful model enzymes, many of these are also of significant utility in industrial biocatalysis and sensing of toxic chemicals, including organophosphate nerve agents.[37,38]

Enzyme Immobilization on Polymer-Modified Nanospheres with Tunable Hydrophobicity. The correlation between optimal brush chemistry and immobilized enzyme activity and stability was enabled via the synthesis of mixed PEGMA/SBMA brushes on silica nanospheres. Random copolymer brushes consisting of varying ratios of PEGMA-to-SBMA were grown from the surface of the nanospheres by activators regenerated by electron-transfer atom-transfer radical polymerization (ARGET ATRP), which provides modest oxygen tolerance. To create brushes with varying ratios of PEGMA-to-SBMA, the PEGMA and SBMA monomers were mixed in reaction in 0:1, 1:3; 1:1, 3:1; and 1:0 ratios (hereafter referred to as 0, 25, 50, 75, and 100% PEGMA, respectively). Additionally, glycidyl methacrylate (GMA) was added at a concentration of 5% molar ratio with respect to the total concentration of SBMA and PEGMA. Notably, GMA contains an epoxide moiety that can react covalently with a broad range of nucleophilic groups (mainly cysteine, lysine, histidine, and tyrosine) on the surface of enzymes.[15,39,40] Characterization of the modified particles by dynamic light scattering revealed that their hydrodynamic radii ranged between 488 and 553 nm compared to 411 nm for the unmodified particles (Figure S1). Given this size range, the thickness of the brushes was significantly greater than the hydrodynamic diameter of the enzymes studied (Figure S2). Additionally, using polymer-modified flat silicon oxide surfaces, we found that the static water contact angle of the brush layer increased systematically from 15° (for 0% PEGMA) to 49° (100% PEGMA) (Figure S3). This finding suggested a systematic increase of hydrophobicity with increasing PEGMA content, which was consistent with previous reports from our group.[31,32] Additionally, X-ray photoelectron spectroscopy of the flat surfaces showed a systematic decrease in the nitrogen and sulfur signals associated with SBMA as the content of PEGMA in the brush layer increased (Figure S4).

Following the preparation of the brush-modified nanospheres, the enzymes were reacted with the epoxide moieties in the brush layer in an aqueous solution at an appropriate pH value (8.7). Apparent enzyme loading on the nanospheres was measured by quantifying the amount of enzyme remaining in the solution after reaction with the nanospheres and applying a mass balance (Table S1). The results of the mass balance

https://doi.org/10.1021/acscatal.3c00264
ACS Catal. 2023, 13, 4304−4315

showed that the loading spanned a wide range, from 0.003 to 4 mg, of enzyme per square meter of the support. Similarly, the specific activity of the supported enzymes spanned 4 orders of magnitude. Based on previous reports that saturated coverage on surfaces is typically in the range of 2−5 mg/m^2,[41,42] our results suggest that thrombin, dAChE4, and HRP were immobilized to the brush at sub-monolayer coverage, whereas all other enzymes were immobilized in the brush layer at approximately monolayer coverage. Given the thickness of the polymer brushes, greater than monolayer coverage was possible but not observed. Because the enzymes may react with the brush through multiple different surface groups, it is plausible that each enzyme is tethered to the brush layer via multipoint covalent attachment, although we expect that there is likely a distribution in the number of tethers per enzyme.

Enzyme Activity and Stability on Mixed PEGMA/SBMA Brush Surfaces. The impact of brush composition on enzyme activity and stability was determined by assaying all eight enzymes at temperatures ranging from 20 to 90 °C in 10 °C increments. Figure 1 shows the results of the temperature-dependent activity assays, which entailed the use of fluorogenic substrates, for the immobilized and free forms of each enzyme. As expected, a strong dependence on the underlying brush composition on activity and stability was observed for many of the enzymes, which is consistent with our prior findings for bacterial lipases. Of particular interest was the fact that this dependence varied significantly between enzymes and in some cases led to substantial enhancements in activity at elevated temperatures. Such a dependence was particularly striking for thrombin, chymotrypsin, HRP, trypsin, and dAChE4, which each exhibited a strong preference for a specific brush composition. For example, thrombin was dramatically stabilized on 0% PEGMA-modified nanospheres, whereas dAChE4 was most stable on 100% PEGMA-modified nanospheres. Additionally, chymotrypsin and HRP exhibited a strong preference for the 50% PEGMA composition and thus favored mixed compositions with moderate hydrophilicity. Notably, the stabilization of thrombin was evident at temperatures as low as 20 °C, where the activity of the immobilized enzyme was 4-fold higher than that of soluble thrombin. While the soluble enzyme was inactivated at 50 °C, the activity of thrombin on 0% PEGMA-modified nanospheres was active up to 90 °C with an optimum temperature (T_{opt}) at 80 °C (Figure 2). This represents a remarkable shift in T_{opt} of 50 °C with respect to soluble thrombin. Additionally, at this T_{opt}, the maximum activity of thrombin on 0% PEGMA-modified nanospheres (V_{opt}) was 20-fold greater than that for soluble thrombin at its original T_{opt}. In the case of dAChE4, a similar increase in activity at low temperatures was observed upon immobilization on 100% PEGMA-modified nanospheres compared to other brush compositions as well as soluble dAChE4. The apparent increase in thermal stability also led to a 20 °C increase in T_{opt} (from 40 to 60 °C) relative to soluble dAChE4 as well as a 10-fold increase in V_{opt} and significant retention of activity up to 90 °C. Likewise, the T_{opt} value for both chymotrypsin and HRP increased by 10 °C, respectively, upon immobilization on 50% PEGMA-modified nanospheres relative to their soluble counterparts. Although the increase in V_{opt} was less significant or non-existent for trypsin and hCAII, similar stabilizing effects as a function of brush composition were observed. For hCAII, it is perhaps unsurprising that a large stabilization effect was not observed since this form of carbonic anhydrase was previously engineered to be highly thermostable.[43]

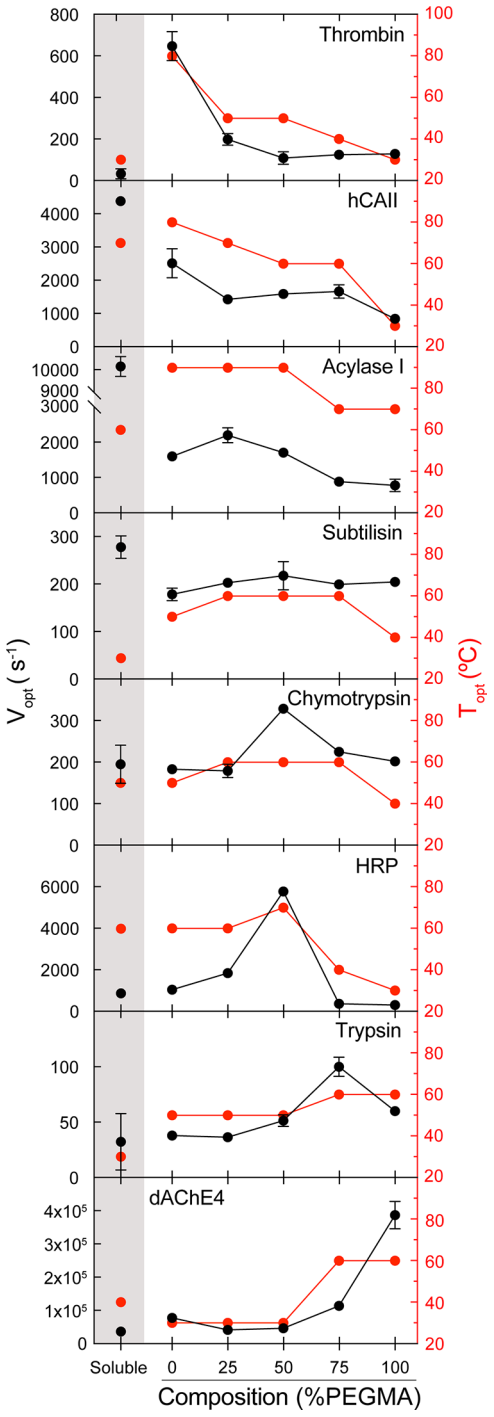

Figure 2. Optimal activity (V_{opt}) and temperature (T_{opt}) of each immobilized enzyme as a function of polymer brush composition. The data points in the shaded region correspond to the V_{opt} and T_{opt} values of the soluble forms of each enzyme. Error bars of V_{opt} represent the standard error of the mean for three technical replicates (n = 3).

While the stability of most of the enzymes tested was strongly dependent on brush composition, a subset of the enzymes appeared to be largely insensitive to the brush chemistry. This was particularly apparent for acylase I and subtilisin Carlsberg, where the activity of the immobilized enzymes as a function of temperature was independent of the

https://doi.org/10.1021/acscatal.3c00264
ACS Catal. 2023, 13, 4304−4315

composition of the underlying brush. For example, acylase I exhibited similar activity for all brush compositions across the 20−70 °C range, although compositions of 0−50% PEGMA were most stabilizing above 70 °C. The dramatic decrease in activity for immobilized relative to soluble acylase I may also be explained by the immobilization of the enzyme as a monomer. While the monomeric form of the enzyme is still active, it has been shown that the activity of the monomeric form of the enzyme is less than that of the native dimer of the enzyme in solution. Similarly, the differences in the activity of immobilized subtilisin Carlsberg across the composition of brushes was negligible at all temperatures. However, despite the lack of dependence on brush composition, it was notable that the T_{opt} for immobilized subtilisin Carlsberg was markedly higher than that for soluble subtilisin. This increase in T_{opt} is significant since maintaining protease activity at high temperatures may improve the activity toward unfolded proteins, which were not used here (note: enzyme activity was measured using a fluorescent small molecule substrate rather than a peptide substrate).

A summary of the effect of brush composition on the T_{opt} and V_{opt} of all eight enzymes is shown in Figure 2. From the plots of T_{opt} and V_{opt} versus brush composition, differences in the strength of the dependence on brush composition for the enzymes are readily apparent. For enzymes such as thrombin and hCAII, a clear systematic decrease in stability with increasing PEGMA content in the brush layer can be observed. Conversely, the opposite effect can be observed for dAChE4, where the enzyme was apparently destabilized by the presence of the zwitterionic monomer. These results underscore that the effects of enzyme immobilization on stability and activity are strongly specific to the enzyme−brush interface. Moreover, while demonstrating the importance of rationally tuning the enzyme−polymer brush interface, our findings highlight the need for a nuanced approach to estimate a priori the effect of polymer brush composition on the activity and stability of immobilized enzymes.

Multivariate Vectorial Analysis of Immobilized Enzyme Activity. When analyzing the performance of an immobilized enzyme as a systematic function of a relevant variable, such as brush composition, it is desirable to determine not only the optimal value of the variable but the degree to which that value is preferred. Here, we developed and employed a multivariate method and a vectorial visualization scheme that defined both the preferred support composition and the extent to which the preference was negligible or pronounced. To pursue this, for each temperature at which activity was measured, the activity of each enzyme when immobilized on each support was represented as a vector (Figure 3). Since five polymeric compositions were used in this study (0, 25, 50, 75, and 100% PEGMA), the vectors point to the five apexes of a regular pentagon. While the angular direction of each vector reflects the composition of the relevant brush support, the modulus of each vector reflects the activity of the enzyme that is immobilized on that support. Upon vectorial summation and normalization of the modulus of the resulting vector to the sum of the activity vector magnitudes, a "preference vector" ($\vec{V}_P$) is obtained where the angular component of $\vec{V}_P$ represents the apparent preferred support composition of the enzyme for that temperature (Ω) and the modulus represents the magnitude of the preference of the enzyme to a support composition, or "preference index" (ρ).

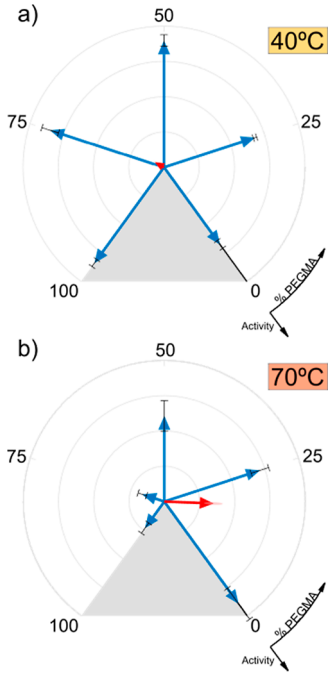

Figure 3. Representative vector plots for immobilized hCAII at 40 (a) and 70 °C (b) on mixed PEGMA/SBMA brushes (marked by dashed lines in Figure 1). Each blue vector represents the activity of hCAII when immobilized on a support of a particular composition. The modulus of the vector represents the enzymatic activity, and the azimuthal angle represents the composition of the copolymer brush support in terms of % PEGMA. The red vector represents the preference vector ($\vec{V}_P$), whose coordinates are found by vectorial summation of blue vectors. Error bars of blue vectors represent the standard error of the mean for three technical replicates (n = 3). The red ellipse in the preference vector represents the uncertainty of $\vec{V}_P$ in the radial and angular directions, whose determination is described in the Materials and Methods section.

Notably, ρ can vary between 0 and 1, where 0 represents no preference to any brush support and 1 represents a strong preference to the support composition indicated by the direction of $\vec{V}_P$. Figure 3a shows an example of a vector plot for the activity of immobilized hCAII at 40 °C, where the enzyme has approximately equal activity for all brush compositions. As a result, the activity vectors are nearly identical in magnitude, and upon performing the vectorial summation, $\vec{V}_P$ has a modulus close to 0, which indicates that hCAII has no preference to any polymer brush support at 40 °C. This vectorial analysis clearly depicts situations where thermal denaturation effects are significant, and an enzyme is better stabilized against denaturation by some supports than by others. Notably, the activity of immobilized hCAII at 70 °C was highest on 0% PEGMA (Figure 3b) and lower on all other supports, with decreasing activity as the relative fraction of PEGMA increased. After vectorial summation to obtain $\vec{V}_P$ at 70 °C, it was observed that ρ had a substantial magnitude (ρ = 0.349), and $\vec{V}_P$ pointed to a support of high hydrophilicity (Ω = 18% PEGMA). While demonstrating the preference for hCAII at 70 °C for hydrophilic supports, this illustrates the type of information that can be obtained from this analysis.

Vectorial analysis of the activity of each immobilized enzyme at their respective T_{opt} clearly revealed the preference (or lack thereof) of each enzyme for a particular brush composition

https://doi.org/10.1021/acscatal.3c00264
ACS Catal. 2023, 13, 4304−4315

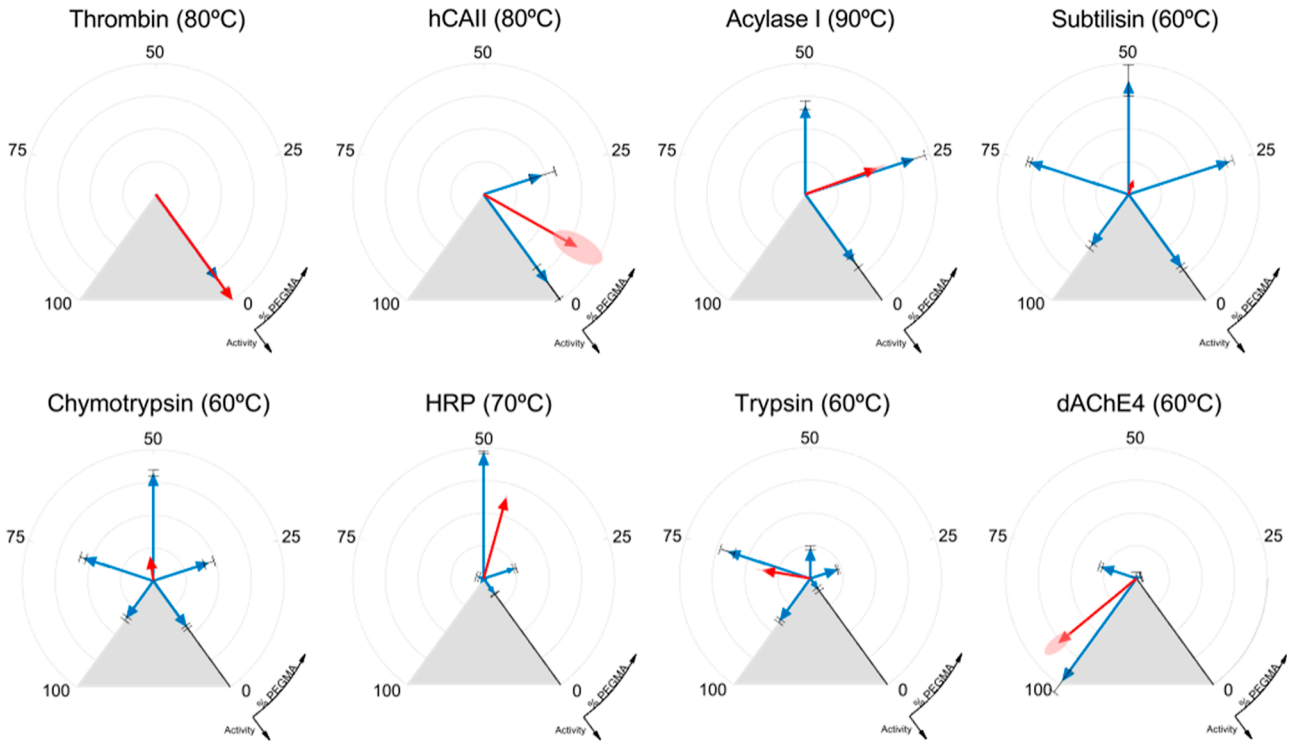

Figure 4. Vector plots for all the eight immobilized enzymes at their respective T_{opt} values. The angular component of the preference vector (in red) moves from polymeric supports of low PEGMA content to polymeric supports of high PEGMA content as overall hydrophobic intensity ($\Delta G^{solv,total}$/area) increases as determined via Hi-patch analysis. Error bars of blue vectors represent the standard error of the mean for three technical replicates (n = 3). The red ellipse in the preference vector represents the uncertainty of $\vec{V}_P$ in the radial and angular directions (described in the Materials and Methods section). Due to the variable degree of uncertainty, the ellipse is not visible for several of the immobilized enzymes.

(Figure 4). It was observed that $\vec{V}_P$ systematically rotated across the range of polymer support compositions as a function of hydrophobic intensity of the enzyme surface. Specifically, as $\Delta G^{solv,total}$/area increased for the enzymes (from Table 1), the value of Ω generally increased from 0% PEGMA (for thrombin) to ∼95% PEGMA (for dAChE4). This is consistent with our hypothesis that hydrophobic enzymes prefer more hydrophobic supports, while more hydrophilic enzymes prefer more hydrophilic supports. Notably, while thrombin, hCAII, acylase, HRP, and dAChE4 had values of $\rho > 0.5$, the values of ρ for subtilisin and chymotrypsin were 0.12 and 0.19, respectively. Furthermore, we found it instructive to visualize the results of this analysis as a function of temperature. For each enzyme, the ρ and Ω components of $\vec{V}_P$ at each temperature were plotted as a trajectory in Figure S5. In each plot, a noise threshold was determined, which was based on the pooled standard error in ρ for all data points associated with a given enzyme. Data points above this threshold were used to calculate the weighted preferred support composition ($\bar{\Omega}$) for each enzyme (Table 2), in which the preferred support composition Ω was weighted by the degree of preference ρ and whose value covered the entirety of the SBMA/PEGMA copolymer composition range.

Correlation between Enzyme Hydrophobicity and Polymeric Support Composition. To ultimately answer the question of whether the enzyme surface hydrophobicity can be used to guide the design of stabilizing brush supports for any given enzyme, the relationship between $\Delta G^{solv,total}$/area and $\bar{\Omega}$ for all the eight enzymes was analyzed and is shown in Figure 5. This plot includes $\Delta G^{solv,total}$/area and $\bar{\Omega}$ from the re-analysis of the four bacterial lipases [*Bacillus subtilis* lipase A (LipA), *Rhizomucor miehei* lipase (RML), *Candida rugosa* lipase (CRL), and *C. antarctica* lipase B (CALB)] used in our previous work.[31] Notably, using our vectorial analysis approach, we determined that the values of $\bar{\Omega}$ for LipA, RML, CRL, and CALB were 1.52, 13.37, 53.80, and 97.71% PEGMA, respectively. Although these lipases were immobilized on the brush supports using a different covalent tethering chemistry (i.e., via *N*-hydroxysuccinimidyl groups in the brush layer instead of epoxide groups), the use of a different tethering chemistry is unlikely to affect $\bar{\Omega}$. Remarkably, our results show a nuanced and overall linear correlation between $\Delta G^{solv,total}$/

Table 2. Weighted Preferred Support Composition ($\bar{\Omega}$) of Enzymes in This Study[a]

enzyme	$\bar{\Omega}$ (% PEGMA)
thrombin	1.28 ± 3.05
hCAII	6.13 ± 4.00
acylase I	25.5 ± 6.7
subtilisin	38.4 ± 8.5
HRP	41.7 ± 5.5
chymotrypsin	46.8 ± 3.0
trypsin	79.4 ± 8.1
dAChE4	93.9 ± 7.6
LipA[b]	1.52 ± 2.39
RML[b]	13.4 ± 2.9
CRL[b]	53.8 ± 8.4
CALB[b]	97.7 ± 47.3

[a]Error represents the propagated error from the calculation of $\bar{\Omega}$ as described in the Materials and Methods section. [b]$\bar{\Omega}$ was determined via re-analysis of activity plots from ref 31 using the vector-based method.

https://doi.org/10.1021/acscatal.3c00264
ACS Catal. 2023, 13, 4304−4315

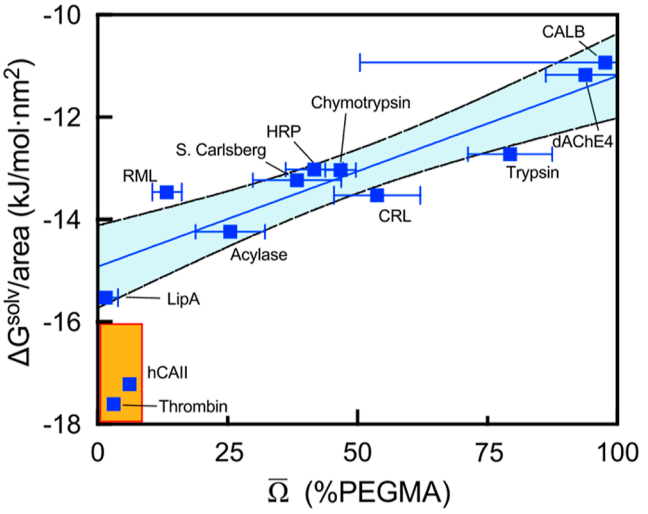

Figure 5. Linear correlation between $\Delta G^{solv,total}$/area and $\bar{\Omega}$ for the eight enzymes used in this study as well as the bacterial lipases used in previous studies.[31] The data points in the orange box represent enzymes of extreme hydrophilicity that are optimally stabilized in 0% PEGMA supports, which were not accounted for the linear fit. Error bars represent the propagated error related to the calculation of $\bar{\Omega}$ from data points from Figure S5. Confidence bands represent the 95% confidence interval associated with the linear fit.

area and $\bar{\Omega}$ (over the accessible range of $\bar{\Omega}$), which suggested that $\Delta G^{solv,total}$/area as a single parameter was sufficient to guide the choice of polymer brush supports to stabilize the enzyme. This is particularly remarkable when considering how complex and different the structure and surface of each enzyme are. Furthermore, it is notable that this correlation was approximately linear over a broad range of enzyme surface hydrophobicity and covered the entire range of brush compositions (from 0 to 100% PEGMA). An apparently linear correlation between $\Delta G^{solv,total}$/area and $\bar{\Omega}$ was observed between −16 and −10 kJ/mol·nm^2, and the two enzymes with $\Delta G^{solv,total}$/area less than −16 kJ/mol·nm^2 were also optimally stabilized in highly hydrophilic supports but were not within the linear range of this correlation. These observations suggest that the range of application of the approximately linear correlation is limited by the hydrophilicity of the homopolymeric supports (i.e., 0 and 100% PEGMA) and could potentially be extended by using more hydrophilic and/or hydrophobic polymers, which have been described elsewhere.[44] Notably, for the specific copolymer mixture employed in this study, the correlation suggests that enzymes outside the linear range on the hydrophilic side (i.e., with $\Delta G^{solv,total}$/area < −16 kJ/mol·nm^2) will be optimally stabilized by 0% PEGMA supports, which was indeed observed for thrombin and hCAII. Conversely, we expect that exceptionally hydrophobic enzymes (i.e., more hydrophobic than dAChE4 and CALB) will be optimally stabilized by 100% PEGMA supports since the PEGMA homopolymer represents the boundary of maximal support hydrophobicity in this study. Overall, our findings illustrate the potential of enzyme surface hydrophobicity as a parameter to inform the choice of brush composition for a given enzyme. This in turn has immense practical implications in rationally tailoring polymeric supports for enzymes without requiring intensive empirical trial and error experimentation.

As further evidence of the importance of $\Delta G^{solv,total}$/area towards determining approximate $\bar{\Omega}$, our results show that two of the enzymes used in this study −−dAChE4 and CRL−− can have very different $\bar{\Omega}$ values with similar tertiary structures. In particular, the tertiary structures of dAChE4 and CRL are nearly identical, with a C_α root-mean-square deviation between their structures 1.319 Å (Supporting Information Appendix, Figure S6a). Using Hi-patch, we found that structurally, the only difference between the enzymes was the presence of a large hydrophobic patch in dAChE4 of 600 Å^2, which was not present on the surface of CRL (Figure S6b,c). Interestingly, the presence of this large hydrophobic patch alone led to a dramatic increase in $\Delta G^{solv,total}$/area from −13.5 kJ/mol·nm^2 for CRL to −11.2 kJ/mol·nm^2 for dAChE4. Because the structures of the enzymes are nearly identical, the difference in $\bar{\Omega}$ (53.8% PEGMA for CRL and 93.9% PEGMA for dAChE4) may be attributed to the difference in $\Delta G^{solv,total}$/area and not differences in the tertiary structure of these two enzymes. While these observations suggest that polymer preference is not affected by enzymes' tertiary structure, they are based on one pair of enzymes and hence not generalizable. Nonetheless, we found that it is important to consider the quaternary structure of the enzymes, including for dAChE4 and acylase I, which are dimers in solution. Notably, the $\Delta G^{solv,total}$/area of the native dimeric form of dAChE4 and acylase I was −15.4 and −16.0 kJ/mol·nm^2, which was considerably lower than that of the monomers for each enzyme. This was likely due to the occlusion of the hydrophobic patches at the dimer interface in the analysis of the monomers. Interestingly, the value of $\Delta G^{solv,total}$/area for the monomeric enzymes was in good agreement with the rest of the linear correlation between the enzymes and supports. This was consistent with expectations associated with the immobilization conditions, in which the monomeric form was favored via addition of the non-ionic surfactant, and re-dimerization was prevented due to immobilization.

CONCLUSIONS

Our results demonstrate a remarkable correlation between immobilized enzyme surface hydrophobicity and the optimal brush composition of mixed PEGMA/SBMA surfaces. By demonstrating that this correlation extends to a broad range of structurally and functionally diverse enzymes that are also non-related, these results build on our prior findings and demonstrate the broad applicability of this correlation. At a molecular level, our findings show that the optimal brush composition for any given enzyme can be informed by the single parameter $\Delta G^{solv,total}$/area. This itself is extraordinary given the complexities of the structure of enzymes and the role of different types of non-covalent interactions in stabilizing proteins, which would seem to suggest that other parameters may also be important. Interestingly, our results further showed how two enzymes with similar tertiary structures, but different $\Delta G^{solv,total}$/area can have very different optimal brush compositions. This was specifically shown by comparing $\Delta G^{solv,total}$/area and the optimal brush compositions for dAChE4 and CRL, which ultimately had very different $\bar{\Omega}$ values. While these findings demonstrate the utility of $\Delta G^{solv,total}$/area as a guide for choosing stabilizing brush compositions, it remains to be seen if the mechanisms of stabilization by which enzymes are preferentially stabilized on specific brush compositions are the same or enzyme-specific. Additionally, for enzymes that are more hydrophilic than the

https://doi.org/10.1021/acscatal.3c00264
ACS Catal. 2023, 13, 4304−4315

most hydrophilic supports used here, it is interesting to characterize their stability on surfaces that are even more hydrophilic, potentially including other zwitterionic polymers [e.g., poly(carboxybetaine methacrylate)] or sugar-mimicking polymers [e.g., poly(glycosyloxyethyl methacrylate)]. Finally, investigation of increasingly complex heterogeneous materials, containing aromatic, anionic and/or cationic, branched aliphatic, or strongly hydrophilic non-charged monomers, remains unexplored, particularly in their interaction with extremely complex protein surfaces. Future work will aim to dissect the role of interactions from each of these classes of monomers on macroscopic activity, as well as the underlying mechanisms that can lead to stabilization or destabilization. Given the utility of $\Delta G^{solv,total}$/area for guiding brush design, our findings have immense implications in developing complex synthetic materials that dramatically improve the stability of enzymes in extreme environments where it may be desirable to use enzymes for industrial and/or biotechnological applications.

MATERIALS AND METHODS

Materials. Copper (II) bromide, *N*,*N*,*N*′,*N*″,*N*″-pentamethyldiethylenetriamine (PMDETA), L-ascorbic acid, poly(ethylene glycol) methyl ether methacrylate (M_n = 300 Da, PEGMA), tetraethyl orthosilicate, ammonium hydroxide (30% in water), anhydrous toluene, methanol, *N*,*N*′-dimethylformamide (DMF), bicine, sodium pyrophosphate, and 4-methylumbeniferyl acetate were purchased from Sigma-Aldrich Millipore (St. Louis, MO). [(2-Methacryloyloxy)ethyl]-dimethyl-(3-sulfopropyl)-ammonium hydroxide (SBMA) and 2,2,2-trifluoroethanol were purchased from TCI Chemicals (Portland, OR). (*p*-Chloromethyl)phenyltrichlorosilane (CMPS) was purchased from Gelest (Morrisville, PA). *N*-Octylglucoside was purchased from Research Products International (Mount Prospect, IL). Glycidyl methacrylate (GMA) was purchased from MP Biomedicals LLC (Irvine, CA). 4-Methylumbelliferyl 4-guanidinobenzoate was purchased from Abcam (Cambridge, UK). Amplex Red was purchased from Thermo Fisher (Waltham, WA). All chemical reagents were used without further purification. Additionally, chymotrypsin from bovine pancreas, trypsin from porcine pancreas, acylase I from porcine kidney, subtilisin Carlsberg from *Bacillus licheniformis*, horseradish peroxidase, and thrombin from bovine plasma were also purchased from Sigma-Aldrich Millipore (St. Louis, MO), while human carbonic anhydrase II (hCAII) and expression-optimized acetylcholinesterase (dAChE4) were expressed recombinantly (see below).

Expression of hCAII and dAChE4 and Enzyme Purification. Recombinant hCAII in a pET28b+ vector (kindly provided by Ryan Mehl, Oregon State University) was expressed in *E. coli* BL21(DE3) as described previously.[24,43] For expression of dAChE4, the gene encoding the enzyme was provided by Sarel Fleishman in a pET32b+ vector (Addgene entry #83917) and transformed into *E. coli* Shuffle T7 express cells.[36] After transformation of the vector, a single colony was selected in an ampicillin-supplemented LB agar plate and grown overnight in LB medium supplemented with 100 μg/mL ampicillin. The overnight culture was used to inoculate 250 mL of 2xYT medium with 100 μg/mL ampicillin and 1% (v/v) sterilize-filtered ethanol in which the enzyme was expressed for 20 h at 16 °C after induction with isopropyl β-D-1-thiogalactopyranoside to a final concentration of 0.2 mM. Following expression, the cells were harvested via centrifugation at 8000×*g* at 4 °C and subsequently flash-frozen and stored in −80 °C. For purification, the frozen cells were resuspended in chilled lysis buffer (20 mM Tris, 100 mM sodium chloride, 10% glycerol, 0.1% w/v *n*-octylglucoside, 20 mM imidazole, and pH 8) and sonicated for 5 min in ice. After lysis, the lysate was centrifuged at 12,000×*g* for 1 h at 4 °C, and the clarified lysate was filtered using a 0.45 μm filter and loaded on a Bio-Rad nickel-IMAC cartridge. After elution with 300 mM imidazole, dAChE4 was buffer-exchanged into immobilization buffer using a Bio-Scale Mini Bio-Gel 50 mL P-6 desalting cartridge (Bio-Rad, USA). Similarly, the other enzymes were also buffer-exchanged into their respective immobilization buffers as summarized in Table S2, which also helped to remove any excipients. The final concentration of each enzyme was quantified by measuring absorbance at 280 nm via UV/vis using their appropriate extinction coefficients based on their sequence.

Functionalization of Silica Nanoparticles. Silicon oxide monodisperse nanospheres were synthesized using the Stöber method.[45] Briefly, 75 mL of tetraethyl orthosilicate was dissolved in a mixture of 768 mL of methanol and 768 mL of ethanol, after which 389 mL of ammonium hydroxide (30% in water) was added dropwise for 5 min with vigorous stirring. After allowing the reaction to proceed at room temperature for 4 h since the addition of the last drop, particles were separated via centrifugation and washed with water (×2), ethanol, and methanol before storing them in a desiccator until further use. 25 g of these particles was treated in a UV−ozone cleaner for 1 h. Subsequently, these particles were suspended in toluene (200 mL), sonicated for 1 min, and reacted with CMPS (200 μL) for 45 min with moderate stirring. Modified particles were then separated via centrifugation and washed with toluene (×2), 2-propanol, water, and 2-propanol and stored in a desiccator. The resulting particles were characterized via dynamic light scattering (Anton Paar Litesizer 500) after resuspension in microfiltered 50 mM sodium phosphate buffer at pH 7.5.

Mixed PEGMA/PSBMA brushes were grafted from the surface of the initiator-modified particles via Activators ReGenerated by Electron Transfer Atom Transfer Radical Polymerization (ARGET ATRP).[2,46−48] Briefly, CMPS-functionalized nanospheres (4 g) were added to Schlenk flasks containing 0−100% PEGMA (with the complementary percentage consisting of SBMA) with 5% glycidyl methacrylate (42.1 μL), 11.2 mg of L-ascorbic acid, and a small copper wire in 20 mL of a 70:30 (v/v) mixture of methanol and DMF. A stock solution with copper and ATRP ligand was made separately, containing 0.0426 g of copper (II) bromide, 398 μL of PMDETA, 210 mL of methanol, and 90 mL of DMF. All solutions were degassed in Schlenk flasks by repeated freeze−pump−thaw cycles (5×). The copper and ligand-containing solution (10 mL) was transferred to the flask containing the nanospheres and monomer mixture under nitrogen to a final volume of 30 mL, which was allowed to react for 1 h at a positive nitrogen pressure of 5 psi. The final concentration of copper was 15 ppm, and molar ratios of all other chemicals are summarized in Table S3. Polymer brush-coated nanospheres were separated via centrifugation, sequentially washed with methanol, DMF, 2,2,2-trifluoroethanol, and methanol, and stored in a desiccator until further use. The size of each composition of brush-functionalized nanospheres was measured via DLS after suspension in microfiltered 50 mM sodium

https://doi.org/10.1021/acscatal.3c00264
ACS Catal. 2023, 13, 4304−4315

phosphate buffer at pH 7.5, after 2 min of probe sonication in ice.

The same polymer brush synthesis process was carried out on flat silicon oxide surfaces (Wafer Pro, Santa Clara, CA). A custom-made goniometer was used to measure sessile drop contact angles of the air−water surface, and the contact angle of these functionalized flat surfaces was analyzed using First Ten Angstroms software (FTA32, Portsmouth, VA). Additionally, chemical characterization of the functionalized flat surfaces was performed using X-ray photoelectron spectroscopy (XPS) with a Kratos AXIS Supra XPS instrument, using an X-ray beam with an acquisition dwell time of 3000 ms at a pressure of 1.8 to 2.3 × 10^{-8} Torr.

Enzyme Immobilization. To enable immobilization, a solution of each enzyme (1.8 mL) was incubated with the polymer brush-coated nanospheres (200 mg) using a revolving orbital shaker. For HRP, the enzyme was allowed to react for 24 h at room temperature, while all the other enzymes were incubated for 36 h at 4 °C. After immobilization, enzyme loading on the particles was determined using a mass balance based on the relative activity of each enzyme remaining in the supernatant of the reaction. The relative activity was calculated by normalizing the activity of the enzyme in the supernatant to the activity of the enzyme in the absence of particles. In the case of HRP, enzyme loading was cross-verified by UV/vis spectroscopy by measuring absorption of the heme group at 403 nm, whose extinction coefficient at 403 nm is 1.02 × 10^5 M^{-1} cm^{-1}.[49] To ensure that any non-covalently adsorbed enzyme was removed from the polymer brush layer, the particles were washed multiple times with fresh reaction buffer until the enzymatic activity of the supernatant was negligible.

Activity Assays. The enzyme activity was assayed by monitoring the initial rate of the reaction of fluorogenic substrates for each enzyme. For thrombin, subtilisin, trypsin, and chymotrypsin, the activity was determined by monitoring the hydrolysis of 4-methylumbelliferyl 4-guanidinobenzoate (200 μM in reaction) using excitation and emission wavelengths of 365 and 444 nm, respectively. For HRP, the oxidation of Amplex Red (25 μM in reaction) was monitored using excitation and emission wavelengths of 570 and 593 nm, respectively, in the presence of 1 mM H_2O_2. For hCAII, acylase I, and dAChE4, the activity was measured using 4-methyllumbeniferyl acetate (0.5 mM in reaction) with excitation and emission wavelengths of 365 and 444 nm, respectively. The assay buffers used for each enzyme are summarized in Table S2. To collect temperature-dependent activity data, a Horiba Scientific FluoroMax-4 spectrofluorometer with a Peltier temperature control system was used. For all experiments, a 1 nm slit width was used for both excitation and emission wavelengths. The rate of product formation was normalized by the concentration of free and immobilized enzyme in each assay. A calibration curve of fluorescence units versus concentration was also prepared for each released fluorophore. Additionally, the background substrate consumption was measured and subtracted from activity measurements at each temperature. For reactions at elevated temperatures, the buffer was preheated to the target temperature in an external water bath.

Vectorial Analysis of Enzyme Activity Data. Temperature-dependent activity profiles were analyzed using a vector-based method. In this method, the enzyme activity for each brush support at a fixed temperature was represented in a polar plot as a vector pointing to the vertex of a pentagon (where the vertices of the pentagon represented each of the brush compositions). Thus, the angular component of each vector represented brush composition, and the radial component represented the enzyme activity. The vectors were subsequently summed (and normalized by the sum of activity vector moduli) to determine the "preference vector" ($\vec{V}_{P,j}$) using the following expression

$$\vec{V}_{P,j} = \frac{\sum_i^n \vec{V}_{i,j}}{\sum_i^n \left\|\vec{V}_{i,j}\right\|}$$

In this expression, $\vec{V}_{i,j}$ denotes the activity vector of a given enzyme when immobilized on support i, the index j represents the discrete values of temperature used in the experiments, and n represents the total number of brush support compositions (i.e., 5). $\vec{V}_{P,j}$ is a vector whose angular direction represents the apparent optimal polymer composition (Ω_j) at temperature j and whose modulus represents the preference index (ρ_j), which could vary between 0 (indicating no preference for a brush support) and 1 (indicating full preference). To estimate the uncertainty of the preference vector ($\mathrm{unc}(\vec{V}_P)$) in the radial ($\mathrm{unc}(\vec{V}_P)|_{radial}$) and angular ($\mathrm{unc}(\vec{V}_P)|_{angular}$) directions, the coordinates and uncertainties of activity vectors $\vec{V}_{i,j}$ were transformed into Cartesian coordinates, where the uncertainty was represented by the standard error of the mean (SEM) of three technical replicates. The uncertainties of each vector $\vec{V}_{i,j}$ in Cartesian coordinates were propagated via summation in quadrature, resulting in the uncertainty of the preference vector in Cartesian coordinates. Previous work from Hall[50] was used as a framework to translate $\mathrm{unc}(\vec{V}_P)$ from Cartesian coordinates to polar coordinates (i.e., uncertainty in the preference index ρ_j and apparent optimal composition Ω_j), using the following matrix expression

$$\boldsymbol{V}_{pol} = \boldsymbol{R}^{-1}\cdot\boldsymbol{V}_{cart}\cdot(\boldsymbol{R}')^{-1}$$

where $\boldsymbol{R}$ is the coordinate rotation matrix, $\boldsymbol{V}_{pol}$ is the covariance matrix in polar coordinates, and $\boldsymbol{V}_{cart}$ is the covariance matrix in Cartesian coordinates. $\boldsymbol{R}$, $\boldsymbol{V}_{pol}$, and $\boldsymbol{V}_{cart}$ are defined as

$$\boldsymbol{R} = \begin{pmatrix} \cos\Omega & -\sin\Omega \\ \sin\Omega & \cos\Omega \end{pmatrix}$$

$$\boldsymbol{V}_{pol} = \begin{pmatrix} \mathrm{unc}^2(\vec{V}_P)|_{radial} & 0 \\ 0 & \mathrm{unc}^2(\vec{V}_P)|_{angular} \end{pmatrix}$$

$$\boldsymbol{V}_{cart} = \begin{pmatrix} \mathrm{unc}^2(\vec{V}_P)|_x & r(x,y)\cdot\mathrm{unc}(\vec{V}_P)|_x\cdot \mathrm{unc}(\vec{V}_P)|_y \\ r(x,y)\cdot\mathrm{unc}(\vec{V}_P)|_x\cdot\mathrm{unc}(\vec{V}_P)|_y & \mathrm{unc}^2(\vec{V}_P)|_y \end{pmatrix}$$

where Ω is the angular component of the preference vector $\vec{V}_P$, $\mathrm{unc}(\vec{V}_P)|_x$ and $\mathrm{unc}(\vec{V}_P)|_y$ are the "x" and "y" Cartesian components of the uncertainty vector $\mathrm{unc}(\vec{V}_P)$, and "$r(x,y)$" is the Pearson coefficient between x and y. Assuming independent variables and no correlation between x and y, the value of $r(x,y)$ was set to 0 and $\boldsymbol{V}_{cart}$ was simplified to

https://doi.org/10.1021/acscatal.3c00264
ACS Catal. 2023, 13, 4304−4315

$$\boldsymbol{V}_{\text{cart}} = \begin{pmatrix} \text{unc}^2(\vec{V}_P)|_x & 0 \\ 0 & \text{unc}^2(\vec{V}_P)|_y \end{pmatrix}$$

Subsequently, $\text{unc}(\vec{V}_P)|_{\text{radial}}$ and $\text{unc}(\vec{V}_P)|_{\text{angular}}$ were calculated as

$$\text{unc}(\vec{V}_P)|_{\text{radial}} = \sqrt{\text{unc}^2(\vec{V}_P)|_{\text{radial}}}$$

$$\text{unc}(\vec{V}_P)|_{\text{angular}} = \tan^{-1}\left[\frac{\sqrt{\text{unc}^2(\vec{V}_P)|_{\text{angular}}}}{\|\vec{V}_P\|}\right]$$

Using these values, the uncertainty of $\vec{V}_P$ in each vector plot was plotted as an ellipse, whose axes corresponded to $\text{unc}(\vec{V}_P)|_{\text{radial}}$ and $\text{unc}(\vec{V}_P)|_{\text{angular}}$, which can be renamed as $\text{unc}(\rho_j)$ and $\text{unc}(\Omega_j)$.

Finally, ρ_j and Ω_j at each temperature were determined from $\vec{V}_{P,j}$ and plotted as a trajectory as shown in Figure S5, and the error bars corresponded to $\text{unc}(\rho_j)$ and $\text{unc}(\Omega_j)$, respectively. In this plot, the mean uncertainty of ρ_j $(\overline{\text{unc}(\rho_j)})$ was calculated, and data points with $\rho_j < (5 \times \overline{\text{unc}(\rho_j)})$ were considered noise and hence not included in subsequent analysis. Last, the weighted preferred composition $(\bar{\Omega})$ was calculated as

$$\bar{\Omega} = \frac{\sum_h \rho_h \cdot \Omega_h}{\sum_h \Omega_h}$$

where h denotes the subset of j temperatures for which ρ_j is above the noise threshold (i.e., $\rho_j > (5 \times \overline{\text{unc}(\rho_j)})$).

■ ASSOCIATED CONTENT

Supporting Information

The Supporting Information is available free of charge at https://pubs.acs.org/doi/10.1021/acscatal.3c00264.

Hydrodynamic diameters of particles, radii of polymer coronas, polymer brush contact angles, XPS spectra of polymer brushes, enzyme support preference plots, structural analyses of CRL and dAChE4, enzyme loading data, buffers utilized, polymerization molar ratios, and AlphaFold2 structure determination (PDF)

■ AUTHOR INFORMATION

Corresponding Authors

Daniel K. Schwartz − *Department of Chemical and Biological Engineering, University of Colorado, Boulder, Colorado 80309, United States;* orcid.org/0000-0001-5397-7200; Phone: (303) 735-0240; Email: daniel.schwartz@colorado.edu; Fax: (303) 492-4341

Joel L. Kaar − *Department of Chemical and Biological Engineering, University of Colorado, Boulder, Colorado 80309, United States;* orcid.org/0000-0002-0794-3955; Phone: (303) 492-6031; Email: joel.kaar@colorado.edu; Fax: (303) 492-4341

Authors

Héctor Sánchez-Morán − *Department of Chemical and Biological Engineering, University of Colorado, Boulder, Colorado 80309, United States;* orcid.org/0000-0002-1505-4058

Luciana Rocha Barros Gonçalves − *Department of Chemical Engineering, Federal University of Ceará, Fortaleza, Ceará 60455-760, Brazil;* orcid.org/0000-0003-0012-8971

Complete contact information is available at: https://pubs.acs.org/10.1021/acscatal.3c00264

Notes

The authors declare the following competing financial interest(s): Although there is no direct conflict of interest, H.S-M, J.L.K and D.K.S. are inventors on a patent application on the use of mixed polymer brush surfaces for stabilizing immobilized enzymes.

MATERIALS AND SOFTWARE AVAILABILITY: All study data are included in the article and/or the Supporting Information. The code for Hi-patch for enzyme hydrophobicity analysis can be found in the Github repository (https://github.com/KaarLab/hi-patch).

■ ACKNOWLEDGMENTS

This work was supported by the NSF (award 2103647) as well as a graduate research fellowship from the NIH Training Grant T32 GM-065103 to H.S-M. L.R.B.G. also received support from the Brazilian research agency CNPq (grant #201509/2019-9). Additionally, the authors thank Ryan Mehl and Sarel Fleishman for providing the plasmids for hCAII and dAChE4, respectively. We are also grateful to Tomoko Borsa for assistance with the acquisition of XPS spectra.

■ REFERENCES

(1) Basso, A.; Serban, S. Industrial applications of immobilized enzymes-A review. *Mol. Catal.* **2019**, *479*, 110607.

(2) Weltz, J. S.; Kienle, D. F.; Schwartz, D. K.; Kaar, J. L. Dramatic Increase in Catalytic Performance of Immobilized Lipases by Their Stabilization on Polymer Brush Supports. *ACS Catal.* **2019**, *9*, 4992−5001.

(3) Chapman, J.; Ismail, A. E.; Dinu, C. Z. Industrial Applications of Enzymes: Recent Advances, Techniques, and Outlooks. *Catalysts* **2018**, *8*, 238.

(4) Nguyen, H. H.; Lee, S. H.; Lee, U. J.; Fermin, C. D.; Kim, M. Immobilized Enzymes in Biosensor Applications. *Materials* **2019**, *12*, 121.

(5) MacConaghy, K. I.; Geary, C. I.; Kaar, J. L.; Stoykovich, M. P. Photonic Crystal Kinase Biosensor. *J. Am. Chem. Soc.* **2014**, *136*, 6896−6899.

(6) Jung, S.; Kaar, J. L.; Stoykovich, M. P. Design and functionalization of responsive hydrogels for photonic crystal biosensors. *Mol. Syst. Des. Eng.* **2016**, *1*, 225−241.

(7) Somu, P.; Narayanasamy, S.; Gomez, L. A.; Rajendran, S.; Lee, Y. R.; Balakrishnan, D. Immobilization of enzymes for bioremediation: A future remedial and mitigating strategy. *Environ. Res.* **2022**, *212*, 113411.

(8) Gao, Y.; Truong, Y. B.; Cacioli, P.; Butler, P.; Kyratzis, I. L. Bioremediation of pesticide contaminated water using an organophosphate degrading enzyme immobilized on nonwoven polyester textiles. *Enzyme Microb. Technol.* **2014**, *54*, 38−44.

(9) Wong, J. K. H.; Tan, H. K.; Lau, S. Y.; Yap, P.-S.; Danquah, M. K. Potential and challenges of enzyme incorporated nanotechnology in dye wastewater treatment: A review. *J. Environ. Chem. Eng.* **2019**, *7*, 103261.

(10) Hartmann, M.; Kostrov, X. Immobilization of enzymes on porous silicas - benefits and challenges. *Chem. Soc. Rev.* **2013**, *42*, 6277−6289.

(11) D'urso, E. M.; Jean-françois, J.; Doillon, C. J.; Fortier, G. Poly(Ethylene Glycol)-Serum Albumin Hydrogel as Matrix for Enzyme Immobilization: Biomedical Applications. *Artif. Cell Blood Substit. Biotechnol.* **1995**, *23*, 587−595.
(12) Wang, Y.; Hsieh, Y.-L. Enzyme immobilization to ultra-fine cellulose fibers via amphiphilic polyethylene glycol spacers. *J. Polym. Sci., Part A: Polym. Chem.* **2004**, *42*, 4289−4299.
(13) Xu, J.; Gao, G.; Duan, L.; Sun, G. Protein and Hydrophobic Association-Regulated Hydrogels with Adhesive Adjustability in Different Materials. *Adv. Mater. Interfac.* **2020**, *7*, 1901541.
(14) González-Sáiz, J. M.; Pizarro, C. Polyacrylamide gels as support for enzyme immobilization by entrapment. Effect of polyelectrolyte carrier, pH and temperature on enzyme action and kinetics parameters. *Eur. Polym. J.* **2001**, *37*, 435−444.
(15) Diamanti, E.; Arana-Peña, S.; Ramos-Cabrer, P.; Comino, N.; Carballares, D.; Fernandez-Lafuente, R.; López-Gallego, F. Intra-particle Macromolecular Migration Alters the Structure and Function of Proteins Reversibly Immobilized on Porous Microbeads. *Adv. Mater. Interfac.* **2022**, *9*, 2200263.
(16) Zucca, P.; Fernandez-Lafuente, R.; Sanjust, E. Agarose and Its Derivatives as Supports for Enzyme Immobilization. *Molecules* **2016**, *21*, 1577.
(17) Pinheiro, B. B.; Rios, N. S.; Rodríguez Aguado, E.; Fernandez-Lafuente, R.; Freire, T. M.; Fechine, P. B. A.; dos Santos, J. C. S.; Gonçalves, L. R. B. Chitosan activated with divinyl sulfone: a new heterofunctional support for enzyme immobilization. Application in the immobilization of lipase B from Candida antarctica. *Int. J. Biol. Macromol.* **2019**, *130*, 798−809.
(18) Ribeiro, E. S.; de Farias, B. S.; Sant'Anna Cadaval Junior, T. R.; de Almeida Pinto, L. A.; Diaz, P. S. Chitosan-based nanofibers for enzyme immobilization. *Int. J. Biol. Macromol.* **2021**, *183*, 1959−1970.
(19) Sweryda-Krawiec, B.; Devaraj, H.; Jacob, G.; Hickman, J. J. A New Interpretation of Serum Albumin Surface Passivation. *Langmuir* **2004**, *20*, 2054−2056.
(20) Park, J. H.; Jackman, J. A.; Ferhan, A. R.; Ma, G. J.; Yoon, B. K.; Cho, N.-J. Temperature-Induced Denaturation of BSA Protein Molecules for Improved Surface Passivation Coatings. *ACS Appl. Mater. Interfaces* **2018**, *10*, 32047−32057.
(21) Chen, J.-W.; Wu, W.-T. Regeneration of immobilized Candida antarctica lipase for transesterification. *J. Biosci. Bioeng.* **2003**, *95*, 466−469.
(22) Sheldon, R. A. Enzyme Immobilization: The Quest for Optimum Performance. *Adv. Synth. Catal.* **2007**, *349*, 1289−1307.
(23) Faulón Marruecos, D.; Kastantin, M.; Schwartz, D. K.; Kaar, J. L. Dense Poly(ethylene glycol) Brushes Reduce Adsorption and Stabilize the Unfolded Conformation of Fibronectin. *Biomacromolecules* **2016**, *17*, 1017−1025.
(24) Chaparro Sosa, A. F.; Bednar, R. M.; Mehl, R. A.; Schwartz, D. K.; Kaar, J. L. Faster Surface Ligation Reactions Improve Immobilized Enzyme Structure and Activity. *J. Am. Chem. Soc.* **2021**, *143*, 7154−7163.
(25) Weltz, J. S.; Schwartz, D. K.; Kaar, J. L. Surface-Mediated Protein Unfolding as a Search Process for Denaturing Sites. *ACS Nano* **2016**, *10*, 730−738.
(26) Kienle, D. F.; Falatach, R. M.; Kaar, J. L.; Schwartz, D. K. Correlating Structural and Functional Heterogeneity of Immobilized Enzymes. *ACS Nano* **2018**, *12*, 8091−8103.
(27) Weltz, J. S.; Kienle, D. F.; Schwartz, D. K.; Kaar, J. L. Reduced Enzyme Dynamics upon Multipoint Covalent Immobilization Leads to Stability-Activity Trade-off. *J. Am. Chem. Soc.* **2020**, *142*, 3463−3471.
(28) Smith, J.; Sprenger, K. G.; Liao, R.; Joseph, A.; Nance, E.; Pfaendtner, J. Determining dominant driving forces affecting controlled protein release from polymeric nanoparticles. *Biointerphases* **2017**, *12*, 02D412.
(29) Cardellini, A.; Jiménez-Ángeles, F.; Asinari, P.; Olvera de la Cruz, M. A Modeling-Based Design to Engineering Protein Hydrogels with Random Copolymers. *ACS Nano* **2021**, *15*, 16139−16148.
(30) Panganiban, B.; Qiao, B.; Jiang, T.; DelRe, C.; Obadia, M. M.; Nguyen, T. D.; Smith, A. A. A.; Hall, A.; Sit, I.; Crosby, M. G.; et al. Random heteropolymers preserve protein function in foreign environments. *Science* **2018**, *359*, 1239−1243.
(31) Sánchez-Morán, H.; Weltz, J. S.; Schwartz, D. K.; Kaar, J. L. Understanding Design Rules for Optimizing the Interface between Immobilized Enzymes and Random Copolymer Brushes. *ACS Appl. Mater. Interfaces* **2021**, *13*, 26694−26703.
(32) Faulón Marruecos, D.; Saleh, L. S.; Kim, H. H.; Bryant, S. J.; Schwartz, D. K.; Kaar, J. L. Stabilization of Fibronectin by Random Copolymer Brushes Inhibits Macrophage Activation. *ACS Appl. Bio Mater.* **2019**, *2*, 4698−4702.
(33) Chaparro Sosa, A. F.; Black, K. J.; Kienle, D. F.; Kaar, J. L.; Schwartz, D. K. Engineering the Composition of Heterogeneous Lipid Bilayers to Stabilize Tethered Enzymes. *Adv. Mater. Interfac.* **2020**, *7*, 2000533.
(34) Chaparro Sosa, A. F.; Kienle, D. F.; Falatach, R. M.; Flanagan, J.; Kaar, J. L.; Schwartz, D. K. Stabilization of Immobilized Enzymes via the Chaperone-Like Activity of Mixed Lipid Bilayers. *ACS Appl. Mater. Interfaces* **2018**, *10*, 19504−19513.
(35) Fleming, P. J.; Fleming, K. G. HullRad: Fast Calculations of Folded and Disordered Protein and Nucleic Acid Hydrodynamic Properties. *Biophys. J.* **2018**, *114* (4), 856−869.
(36) Goldenzweig, A.; Goldsmith, M.; Hill, S. E.; Gertman, O.; Laurino, P.; Ashani, Y.; Dym, O.; Unger, T.; Albeck, S.; Prilusky, J.; et al. Automated Structure- and Sequence-Based Design of Proteins for High Bacterial Expression and Stability. *Mol. Cell* **2016**, *63*, 337−346.
(37) Dhull, V.; Gahlaut, A.; Dilbaghi, N.; Hooda, V. Acetylcholinesterase Biosensors for Electrochemical Detection of Organophosphorus Compounds: A Review. *Biochem. Res. Int.* **2013**, *2013*, 731501.
(38) Liao, S.; Qiao, Y.; Han, W.; Xie, Z.; Wu, Z.; Shen, G.; Yu, R. Acetylcholinesterase Liquid Crystal Biosensor Based on Modulated Growth of Gold Nanoparticles for Amplified Detection of Acetylcholine and Inhibitor. *Anal. Chem.* **2012**, *84*, 45−49.
(39) Mateo, C.; Grazu, V.; Palomo, J. M.; Lopez-Gallego, F.; Fernandez-Lafuente, R.; Guisan, J. M. Immobilization of enzymes on heterofunctional epoxy supports. *Nat. Protoc.* **2007**, *2*, 1022−1033.
(40) Bonollo, S.; Lanari, D.; Vaccaro, L. Ring-Opening of Epoxides in Water. *Eur. J. Org. Chem.* **2011**, 2587−2598.
(41) Mooney, J. F.; Hunt, A. J.; McIntosh, J. R.; Liberko, C. A.; Walba, D. M.; Rogers, C. T. Patterning of functional antibodies and other proteins by photolithography of silane monolayers. *Proc. Natl. Acad. Sci.* **1996**, *93*, 12287−12291.
(42) Fritz, P. A.; Bera, B.; van den Berg, J.; Visser, I.; Kleijn, J. M.; Boom, R. M.; Schroën, C. G. P. H. Electrode Surface Potential-Driven Protein Adsorption and Desorption through Modulation of Electrostatic, van der Waals, and Hydration Interactions. *Langmuir* **2021**, *37*, 6549−6555.
(43) Kean, K. M.; Porter, J. J.; Mehl, R. A.; Karplus, P. A. Structural insights into a thermostable variant of human carbonic anhydrase II. *Protein Sci.* **2018**, *27*, 573−577.
(44) Fromel, M.; Pester, C. W. Polycarbonate Surface Modification via Aqueous SI-PET-RAFT. *Macromolecules* **2022**, *55*, 4907−4915.
(45) Stöber, W.; Fink, A.; Bohn, E. Controlled growth of monodisperse silica spheres in the micron size range. *J. Colloid Interface Sci.* **1968**, *26*, 62−69.
(46) Konkolewicz, D.; Wang, Y.; Zhong, M.; Krys, P.; Isse, A. A.; Gennaro, A.; Matyjaszewski, K. Reversible-Deactivation Radical Polymerization in the Presence of Metallic Copper. A Critical Assessment of the SARA ATRP and SET-LRP Mechanisms. *Macromolecules* **2013**, *46*, 8749−8772.
(47) Kwak, Y.; Magenau, A. J. D.; Matyjaszewski, K. ARGET ATRP of Methyl Acrylate with Inexpensive Ligands and ppm Concentrations of Catalyst. *Macromolecules* **2011**, *44*, 811−819.
(48) Matyjaszewski, K.; Dong, H.; Jakubowski, W.; Pietrasik, J.; Kusumo, A. Grafting from Surfaces for "Everyone": ARGET ATRP in the Presence of Air. *Langmuir* **2007**, *23*, 4528−4531.

https://doi.org/10.1021/acscatal.3c00264
ACS Catal. 2023, 13, 4304−4315

(49) Zhang, Y.; Schmid, Y. R. F.; Luginbühl, S.; Wang, Q.; Dittrich, P. S.; Walde, P. Spectrophotometric Quantification of Peroxidase with p-Phenylene-diamine for Analyzing Peroxidase-Encapsulating Lipid Vesicles. *Anal. Chem.* **2017**, *89*, 5484−5493.
(50) Hall, B. D. Some considerations related to the evaluation of measurement uncertainty for complex-valued quantities in radio frequency measurements. *Metrologia* **2007**, *44*, L62.

https://doi.org/10.1021/acscatal.3c00264
ACS Catal. 2023, 13, 4304−4315